On the use of explainable AI for susceptibility modeling: examining the spatial pattern of SHAP values

Nan Wang[1,2], Hongyan Zhang[1*], Ashok Dahal[3], Weiming Cheng[2,4,5,6], Min Zhao[7,8,9], Luigi Lombardo[3]

Abstract

Hydro-morphological processes (HMP, any natural phenomenon contained within the spectrum defined between debris flows and flash floods) are globally occurring natural hazards which pose great threats to our society, leading to fatalities and economical losses. For this reason, understanding the dynamics behind HMPs is needed to aid in hazard and risk assessment. In this work, we take advantage of an explainable deep learning model to extract global and local interpretations of the HMP occurrences across the whole Chinese territory. We use a neural network architecture and interpret the model results through the spatial pattern of SHAP values. In doing so, we can understand the model prediction on a hierarchical basis, looking at how the predictor set controls the overall susceptibility as well as doing the same at the level of the single mapping unit. Traditional statistical tools usually lead to a clear interpretation at the expense of large performance, which is otherwise reached via machine/deep learning solutions, though at the expense of interpretation. Explainable AI is the key to combine both strengths and in this work, we explore this combination in the context of HMP susceptibility modeling. Specifically, we demonstrate the extent to which one can enter a new level of data-driven interpretation, supporting the decision-making process behind disaster risk mitigation and prevention actions.

Keywords: Hydro-morphological processes; Spatial effects; SHAP; Explainable AI; China

Corresponding author: Hongyan Zhang

E-mail address: zhy@nenu.edu.cn

[1]School of Geographical Sciences, Northeast Normal University, Changchun, 130024, China

[2]State Key Laboratory of Resources and Environmental Information Systems, Institute of Geographic Sciences and Natural Resources Research, Chinese Academy of Sciences, Beijing, 100101, China

[3]University of Twente, Faculty of Geo-Information Science and Earth Observation (ITC), PO Box 217, Enschede, AE 7500, Netherlands

[4]University of Chinese Academy of Sciences, Beijing, 100049, China

[5]Jiangsu Center for Collaborative Innovation in Geographic Information Resource Development and Application, Nanjing, 210023, China

[6]Collaborative Innovation Center of South China Sea Studies, Nanjing, 210093, China

[7]State Key Laboratory of Earth Surface Processes and Resource Ecology, Beijing Normal University, Beijing, 100875, China

[8]Key Laboratory of Environmental Change and Natural Disaster, Beijing Normal University, Beijing, 100875, China

[9]Center for Geodata and Analysis, Faculty of Geographical Science, Beijing Normal University, Beijing, 100875, China

1 Introduction

Hydro-morphological processes (HMP) define a large spectrum of phenomena that include debris flows, debris floods, flash floods, etc., essentially reflecting the dynamics of a mixture of water and debris moving under the effect of gravity. Because of their impulsive and stochastic nature, they can pose a significant threat to most global communities (Kobiyama and Goerl, 2007). As a result, HMP prediction is one the most emergent topics among researchers working on natural hazards (Gariano and Guzzetti, 2016). Historically, this has been attempted and achieved with satisfying results through statistical methods, in the case of debris flows (Carrara *et al.*, 2008), mud flows (Ozdemir, 2009), earth flows (Can *et al.*, 2005), debris floods Santangelo *et al.* (2011), flash floods (Marchi *et al.*, 2010) and even riverine floods (Merz *et al.*, 2009). These approaches share some degree of dissimilarity, but they also have something consistently in common: the need to understand the given HMP under consideration and predict its occurrence probability. The term "understand" here refers to the inference that statistical solutions offer when explaining the distribution of HMP presences and absences in space (or more rarely in space and time) according to a set of predictors (Amato *et al.*, 2019). However, statistical models are not performance-oriented tools, which is the reason why recent advancements in artificial intelligence have produced valid alternatives (e.g., Merghadi *et al.*, 2020). In such cases, machine and deep learning models are employed to maximize the HMP prediction capacity (Kern *et al.*, 2017). However, this happens at the expense of interpretation. In fact, most of the standard machine learning models become so complex that it is impossible to understand why a given probability has been assigned to a given mapping unit (Korup and Stolle, 2014; Goetz *et al.*, 2015). Only in recent years, the computer science community has worked out potential solutions to combine the performance of machine/deep learning and the interpretation of statistical modelling, giving birth to the concept of explainable AI (XAI, Gunning, 2017; Samek *et al.*, 2017). As a result, XAI has started to attract the attention of researchers even in the field of natural hazards, in the hope of performing predictive tasks with high precision but also understanding the processes underlying the observed data (Tehrani *et al.*, 2022; Li, 2022).

The probabilistic estimation of locations prone to experience HMPs is a notion commonly referred to as susceptibility mapping (Guzzetti *et al.*, 2006) and constitutes an integral part of the hazard and risk standard definitions (e.g., Fell *et al.*, 2008; Domeneghetti *et al.*, 2013). In a data-driven context, the susceptibility is usually quantified using statistical models that either linearly or nonlinearly relate the effect of a set of covariates to the distribution of presence/absence hazard data in the study area. The simpler case belongs to the family of Generalized Linear Models (GLMs), which still constitute the most common method in the literature (Reichenbach *et al.*, 2018; Lima *et al.*, 2022). As for more flexible approaches, these are usually built in the framework of Generalized Additive Models (GAMs Brenning, 2008). The regression coefficients estimated for each covariate lead to the model interpretation in both cases. For GLMs, this is done by examining the sign and magnitude of a single regression coefficient (Brenning, 2005; Lombardo and Mai, 2018). In contrast, for GAMs, this is done over a number of regression coefficients that together define a function associated with each covariate (Loche *et al.*, 2022b; Steger *et al.*, 2022). The role of each model component is then interpreted by reading the sign of the coefficients, with positive values indicating a marginal (assuming all other covariates contributions are fixed) increase of the final susceptibility and negative values indicating the opposite (Shirzadi *et al.*, 2017; Loche *et al.*, 2022a). Another appealing advantage of statistical-based models is their capability to capture and display spatial effects (Song *et al.*, 2020), such as spatially varying coefficients models (e.g., Geographically Weighted Regression, Fotheringham *et al.*, 2003) or (e.g., Spatially Varying Regression, Opitz *et al.*, 2022). However, restricted by the data size and the relationships' complexity, statistical models are usually computationally challenging when dealing with big spatial data (Lombardo *et al.*, 2019).

This level of understanding is generally lost in the case of machine learning tools, where the prediction rule becomes so complex that even visualizing it does not really help understand why the stable or unstable label was assigned to a given catchment (e.g., Yeon *et al.*, 2010). In this context, local interpretation methods such as LIME (Local Interpretable Model-agnostic Explanation) (Ribeiro *et al.*, 2016), and SHAP (SHapley Additive exPlanations) (Lundberg and Lee, 2017), offer the opportunity to flexibly model, visualize and interpret complex geographical phenomena. Rather than providing the feature importance for the whole model, local interpretation methods allow giving detailed feature contributions at the level of each mapping unit. As a result, the integration of machine/deep learning tools with locally interpretable techniques has been explored in a number of geographical studies (Li, 2022; Lubo-Robles *et al.*, 2020; Ullah *et al.*, 2023). These achievements open up a new explainable modeling avenue built by computing and visualizing the SHAP patterns in space, and ultimately by interpreting individual predictions.

China has suffered severe destructive HMPs in recent years (see, He *et al.*, 2018; Liu *et al.*, 2018a; Wang *et al.*, 2020). Therefore, it is important to use this unfortunate information and understand which areas may undergo analogous disasters in the years to come. The Chinese geoscientific community has worked together for this objective, producing a number of documents where the susceptibility to HMP has been assessed at various scales (Lin *et al.*, 2022; Wang *et al.*, 2022b). Following the international trends where machine learning solutions are the preferred architectures to solve prediction tasks, most of the national efforts have prioritized performance (e.g., Zhao *et al.*, 2022a). However, seeking model performance only highlights susceptible locations, thus neglecting the required knowledge necessary to understand why HMP may hit specific areas rather than others. In turn, this implies that decision-makers may not be sufficiently supported in planning suitable mitigation actions. For this reason, we test the extent to which deep learning solutions can be explained by examining the SHAP results and their spatial pattern across the whole Chinese territory. Specifically, due to the continental scale of the study area, we opted for a catchment partition, assigning the presence label if at least one HMP has been locally recorded in the Chinese HMP catalogue (more details in Wang *et al.*, 2021). To offer an interactive experience for the reader, we also created a web-GIS platform where our model results can be queried and used to understand the potential of explainable AI tools.

The paper is organized as follows: Section 2 presents the HMP data, the mapping unit and the variables used in this study; Section 3 describes the adopted methodology for the susceptibility model and how to produce interpretable deep learning results. The analytical protocol we implemented is outlined in Section 4, from calibration to performance assessment and model explanation. In Section 5, we explore the implications of local interpretation and the possible improvements to this work. Ultimately, the conclusions are drawn in Section 6.

2 Materials

2.1 HMP inventory

In this work, we accessed the digital collection of HMP records put together thanks to the China National Flash Flood Disasters Prevention and Control Project (see, Liu *et al.*, 2018b, 2021; Xiong *et al.*, 2019, 2020). This project is a large-scale national initiative that has involved many administrations and research centers across China, to collect, standardize and digitize HMP occurrence data in the last fifty years. Here, we selected HMP locations mapped between 1985 and 2015, and only kept the records with a complete metadata description (x,y, and time in year-month-date format). We adopted this filter to remove noisy and imprecise information, leading to 24,956 selected HMPs (Figure 1).

2.2 Mapping units

The choice of a suitable mapping unit boils down to three criteria. The first links the mapping unit to the process one wants to model. For instance, landslides are often modeled at the slope unit scale because half-basins can reflect the morphodynamic response to slope failures (Carrara *et al.*, 1995; Alvioli *et al.*, 2022). Conversely, HMPs can manifest, travel and develop involving whole catchments, thus making these units the most appropriate choice for flow-type hazards (Lin *et al.*, 2021; Wang *et al.*, 2022b).

The second criterion relates to the computational burden a given mapping unit choice inevitably leads to. For instance, choosing an extremely small mapping unit compared to the extent of the study area may lead to data matrices made of several million rows (or billions of elements overall). Such dimensions are computationally challenging and either may end up limiting the complexity of the model one may choose or impose the need for dedicated computational facilities (Lombardo *et al.*, 2020). The third criterion consists of the data aggregation step required for medium to coarse mapping units. Remote sensing technologies lead to characterize the earth's surface on a very fine scale. For instance, global digital elevation models are now expressed at the scale of a few meters (Moreira *et al.*, 2004). As a result, from thousand to million pixels may be contained in a single catchment. Therefore, one usually needs to summarize the distribution of values expressed at the pixel scale to a much coarser hierarchical level (e.g., Jacobs *et al.*, 2020). This is usually done by computing mean and standard deviation values, but one can also opt for a much more detailed quantile description at times (e.g., Camilo *et al.*, 2017).

In this study, we selected a catchment partition, by using the Hydrological data and maps based on Shuttle Elevation Derivatives at multiple Scales (HydroSHEDS database, https://hydrosheds.org/). This data contains several levels of details, from which we selected the 12^{th} level. This resulted in a partition made of 73,587 catchments for the whole Chinese territory. The catchment size spans from 0.1 km^2 to 667 km^2, with an average area of 130 km^2 and a 95% confidence interval of 231 km^2.

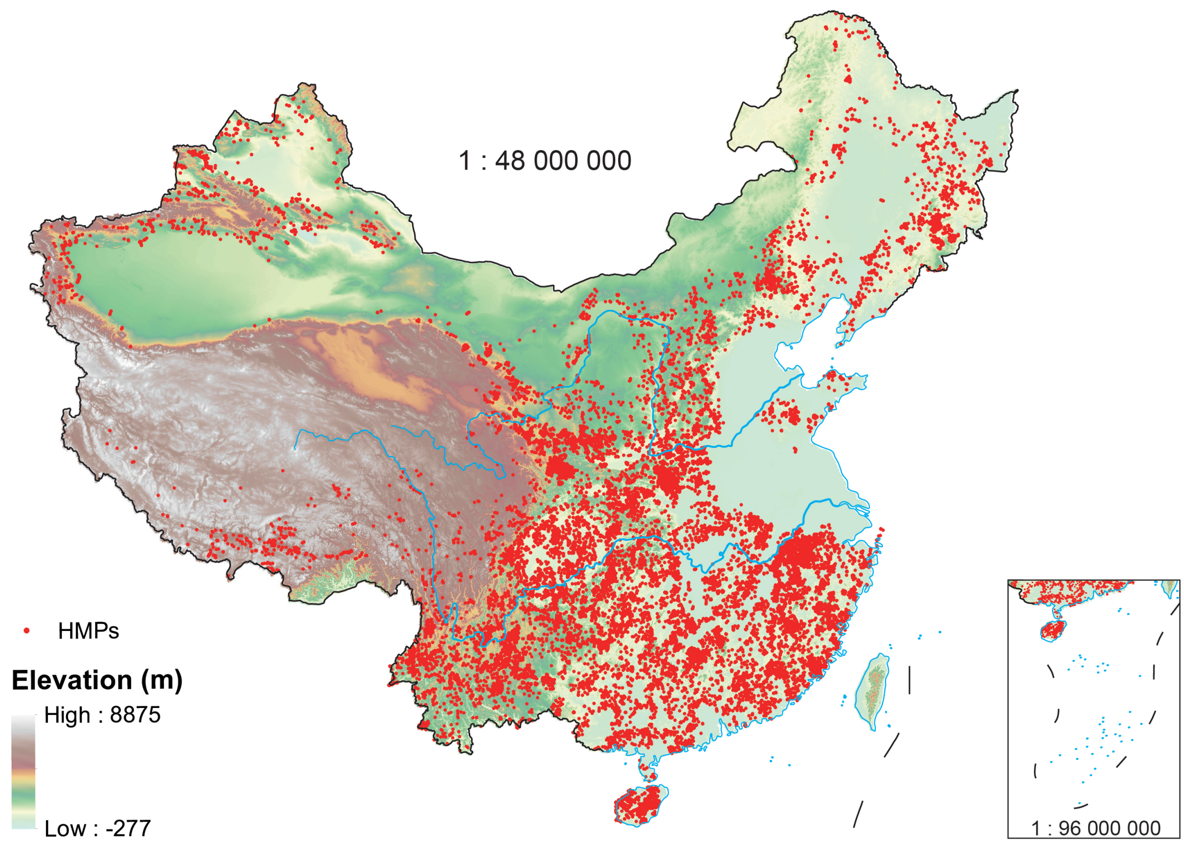

Figure 1: Geomorphological settings of HMPs in China.

2.3 Environmental variables

We chose our predictor set to reflect the environmental conditions responsible for the HMP hazard occurrences, listing terrain, climatic and anthropic influences. As also introduced before, the native covariate resolution differed among covariate groups, and was also inconsistent with respect to the catchment partition. We then adopted the strategy of calculating the mean values per catchment for the following numerical predictors: elevation, slope, planar and profile curvatures. Stream/catchment features (including form factor (Horton, 1932), relief ratio (Schumm, 1956), elongation ratio (Schumm, 1956), and drainage density (Strahler, 1952) are morphometric characteristics representative of the catchment hydrology, thus they did not require any aggregation step. As for NDVI, settlement area and rainfall, these required a dual aggregation step, calculating the respective mean values over 30 years and then per single catchment. Notably, we could have also calculated standard deviation values but the interpretation of such summary statistics becomes very difficult. Because in this work we seek a clear explanation of the predictors' role, we opted to leave out these measures, the additional information they would introduce to the model, and the possible performance increase this would imply. Therefore, we selected a total of 12 variables, whose acronyms and sources are reported in Table 1.

Table 1: Overview of environmental variables used in this study.

Variable	Description	Source
Elv	mean of elevation	SRTM, https://earthexplorer.usgs.gov/
Slp	mean of slope	
Prc	mean of profile curvature	
Plc	mean of plan curvature	
Rr	relief ratio	HydroSHEDS, https://hydrosheds.org/
Ff	form factor	
Er	elongation ratio	
Dd	drainage density	
Wr	wandering ratio	
NDVI	mean of NDVI	GIMMS NDVI, https://data.tpdc.ac.cn/
MaxRain	maximum daily rainfall	Meteorological Data, http://data.cma.cn/
Sa	settlement area	WSF2015, https://developers.google.com/earth-engine/datasets/

3 Methodology

The modeling protocol we followed includes two steps, one where a "black box" neural network is built to produce HMP susceptibility estimates and a second one where the box gets opened for interpretation calculating SHAP values and assessing their spatial patterns per predictor.

These are illustrated in Figure 2, through a general flowchart.

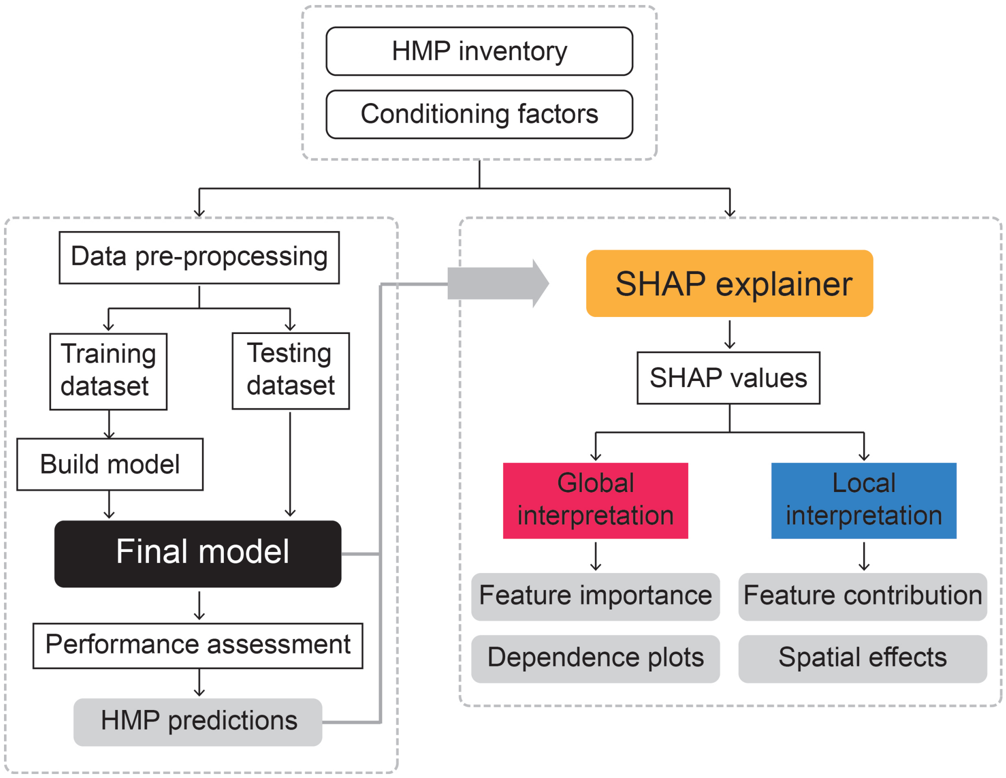

Figure 2: Flowchart of the methodology in this study.

3.1 Susceptibility model

Deep learning models have been proven to be effective in susceptibility modeling in recent studies (Bui *et al.*, 2020; Panahi *et al.*, 2021; Zhao *et al.*, 2022a). To demonstrate the explainability of our model, we opted for an Artificial Neural Networks (ANN; Yilmaz, 2009), although we stress here that SHAP values (the building blocks of explainable AI; Baptista *et al.*, 2022) can be computed even for other data-driven approaches such as random forest (e.g., Titti *et al.*, 2022) or support vector machine (e.g., Yu *et al.*, 2012) to mention a few.

The basic structure of our ANN model consists of nodes and connections that are organized into three layers, i.e., the input layer, the hidden layer, and the output layer. Among them, the hidden layer is used herein to prevent the ANN from falling into bad local minima (De Villiers and Barnard, 1993). In this work, we kept the structure and parameters of the ANN model to be simple, with 12 variables in the input layer, together with 12 hidden layers made out of fully connected layers of size 64 and an output layer with a sigmoid activation function (see, Albawi *et al.*, 2017). We implemented a ReLU non-linear activation and adopted 0.3% dropout in a dropout layer, which could be used to prevent overfitting (see, Li and Yuan, 2017).

As for the explainable component, we used DeepLIFT, and more details are provided in Section 3.2.

3.1.1 Model calibration

We randomly divided the dataset into the training (70%) and testing (30%) parts. In each training epoch, 20% of the training dataset was further randomly selected with replacement to evaluate the training performance. The model was trained via a weighted binary cross-entropy loss function, and some of the important parameters were set as follows:

- optimizer: Adam optimizer
- learning rate: 0.001
- decay steps: 10000
- decay rate: 0.9
- early stopping option: 500

3.1.2 Model validation

The model performance was evaluated on the testing dataset to monitor the generalization ability stemming from the calibration. We recall that the input of a susceptibility model is a vector of presence/absence data, i.e., an array of zeroes and ones. However, the output is not discrete but rather continuously expressed in probabilities. Therefore, to assess the performances of any binary classifier, the first requirement is always the classification of the probability spectrum into a sequence of binary information to be matched against the initial presence/absence observation. This procedure entails the selection of a probability cutoff and for this reason, performance metrics of binary classifiers either fall in the cutoff-dependent or cutoff-independent categories. Here we use both criteria, using a single confusion matrix for the cutoff-dependent analyses. A confusion matrix is made of four elements, reflecting all possible combinations between observed and predicted presence/absence data (Townsend, 1971). As a result, one can define True Positives (TP) and Negatives (TN) for presences and absences that are respectively matched. As for False Positives (FP) and Negatives (FN), these two correspond to model errors, for misclassified absences and presences, respectively. Therefore, it is of utmost importance to select an appropriate probability cutoff, as a wrong choice can drastically change the confusion matrix. For balanced datasets (equal number of presence absences) a straightforward choice is to set the cutoff at 0.5 because the resulting probability distributions are typically bell-shaped. However, in case of unbalanced data, the resulting probability distributions become heavily skewed, with the predominant class pulling the probability spectrum (Ramyachitra and Manikandan, 2014). The latter case is the typical situation one may find in HMP datasets (and luckily for most natural hazards) because the number of occurrences is much lower than the number of absences (Frattini *et al.*, 2010). To address this issue, we opted for a two-stepped approach. The first step is actually part of the model architecture where we used a class-weight binary cross-entropy criterion (Aljohani *et al.*, 2021). This criterion allows one to add a penalty to the model's error measured on the class of interest. In our dataset, the number of absences is approximately seven times the number of presences. Therefore, the model would naturally learn to recognize zeroes (absences) better than ones (presences). However, this issue can be addressed by increasing the weight of the error in the classification of the unstable catchments (by a factor of seven in our case), effectively minimizing the unbalance in the data proportion. In the second step, we a posteriori used a standard procedure based on the Youden Index to select the best probability cutoff (Fluss *et al.*, 2005). We recall here that the Youden Index can be calculated as follows:

$$J = \frac{TP}{TP + FN} + \frac{TN}{TN + FP} - 1 \tag{1}$$

However, even if the retrieved cutoff is the best numerical solution, it still remains only one of the possible solutions. For this reason, we complemented this cutoff-dependent assessment together with Receiver Operating Characteristic (ROC) curves and their integral (AUC) for the cutoff-independent analyses. These curves are generated by plotting pairs of $FP/(FP + TN)$ and $TP/(TP + FN)$ computed for a large number of possible probability cutoffs. As a result, the function linking all pairs sorted by cutoff can be used to calculate its integral, whose resulting value (AUC) indicates how the model performed irrespectively of any specific cutoff. These metrics have then also been assessed over a bootstrapping procedure that randomly selected a 10% subset from the total for further testing.

3.2 Explainable model

The most important goal of explainable deep learning models is to demonstrate how the predictions are reached, highlighting the role (Li, 2022). Shapley values (SHAP), which originated from the game theory, can be used to quantify the contribution of each predictor to the model (Štrumbelj and Kononenko, 2014). Therefore, we computed SHAP **?** for each catchment partitioning the Chinese landscape, allowing to summarize predictors' contributions to the global model and also their relevance at the scale of a single mapping unit. We recall here that SHAP values can be estimated using a number of approaches ranging from Kernel SHAP (e.g., Roshan and Zafar, 2022), Tree SHAP (e.g., Wang *et al.*, 2022a), and Deep SHAP (e.g., Singh *et al.*, 2020). Among these, the latter consists of a high-speed approximation algorithm for SHAP values, whose estimates are reached through a DeepLITF (Deep Learning Important FeaTures) approach (Panati *et al.*, 2022). Specifically, DeepLIFT is a method used for decomposing the output of a neural network on a specific input by back-propagating the contributions of all neurons in the network to each feature of the input (Shrikumar *et al.*, 2017). SHAP values' main strength is to generate locally additive feature attribution via the following equations.

$$\hat{y}_i = shap_0 + shap(X_{1i}) + shap(X_{2i}) + ... + shap(X_{ji}) \tag{2}$$

$$shap_0 = E(\hat{y}_i) \tag{3}$$

where $\hat{y}_i$ is the model prediction for the catchment i, $shap_0$ is the mean value of predictions across all catchments, and $shap(X_{ji})$ is the SHAP values of the j^{th} variable for the catchment i. In this way, the SHAP values start from the initial intercept value $shap_0$, which is the mean value of all predictions, and then add the least contributed term $shap(X_{1i})$, followed by the second least $shap(X_{2i})$, and so on. Finally, the absolute SHAP value reflects each variable's importance for the final prediction (Molnar, 2020).

In this work, we implemented SHAP in open source python package ("shap").

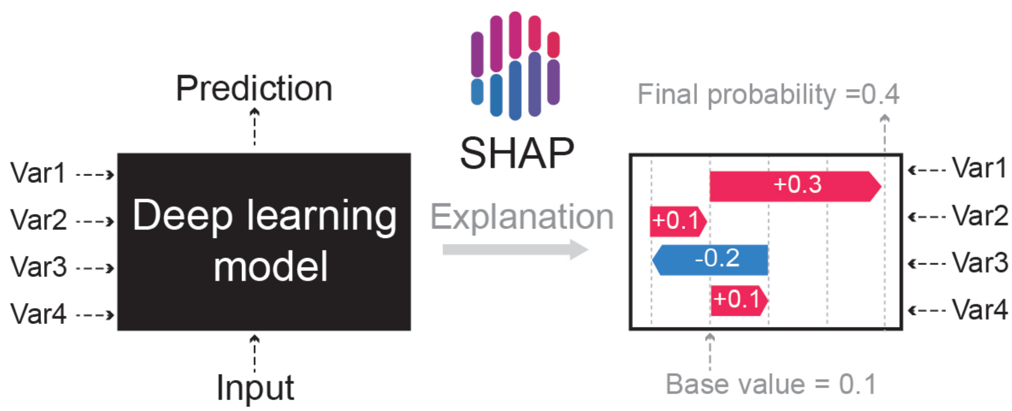

Figure 3: An illustration demonstrating the SHAP-explained deep learning models (modified from Lundberg and Lee (2017)).

4 Results

In this section, we will initially look into an overall assessment of model performance, and later dive into global and local interpretations of the established model. As part of the last procedure, we will also present a step that even other recent explainable AI contributions in natural hazard research have not yet explored. This corresponds to the ability to generate maps of SHAP values for each predictor under consideration. The resulting geographic overview offers a unique perspective on variable contributions and we believe this to be an important element that future explainable AI solutions should be equipped with. This section will be concluded with the estimated susceptibility map.

4.1 Model performance

Our neural network architecture produced performance in the range of excellent results according to the classification system proposed by (Hosmer Jr *et al.*, 2013). This is shown in Figure 4a, where this panel contains both the ROC curves generated from the random cross-validation procedure as well as the AUC values estimated at each bootstrap replicate. The latter is summarized with a boxplot where the median AUC is 0.85, and the two extremes of the AUC distribution are confined above 0.83 and below 0.86. As described in Section 3.1.2, this is a perspective independent of the probability cutoff one may opt for to translate susceptibility values back into presence/absence classes. To complement this assessment, we also report the probability density function of the susceptibility spectrum, together with the estimated Youden Index (Y = 0.52) in Figure 4b. This cutoff leads to the confusion matrix and confusion maps (see also, Nicu *et al.*, 2023) shown in Figure 4c. There, we summarize the frequency distribution for each class of the confusion matrix and plot the corresponding geographic distribution expression across China. We recall here that this confusion matrix relates to the predictive performance assessment. What we observe is that the classification generally reflects the original distribution of presence/absence HMP data, with the dominant class represented by TN. However, the high number of TP (7347 out of 8821 = 83% accuracy) and low number of FN (the complementary 17%) indicate the model's ability to recognize susceptible catchments. In turn, this implies that the FP catchments (15862 out of 64768 = 24%) highlighted in the confusion map may surely be the result of a model error. But, they may also represent locations that the model actually recognizes to likely host HMPs in the future. Answering the question as to whether these FP may be due to misclassification or if they may actually be susceptible but have not yet experienced HMP occurrence is not straightforward. However, examining FP actually constitutes the reason behind susceptibility modeling, and the accuracy we observed in recognizing presence data warrants trusting the model prediction. Notably, these are mostly located in the central and southeast sectors of China.

4.2 Model interpretation

4.2.1 Global interpretation

The most traditional way to understand how a machine-learning models work is to list the variable importance ranking (e.g., Band *et al.*, 2020; Hosseini *et al.*, 2020; Zhao *et al.*, 2022b). Here, we also produce the same graphics in Figure 5 but use SHAP values to sort each predictor according to the impact it may have over the final susceptibility. Among all the variables we considered, NDVI, settlement area, maximum daily rainfall, elevation, and slope steepness appear to be the dominating ones. One of the interesting aspects of using SHAP values instead of traditional variable importance is that SHAP is not bound to positive values, but it ranges from negative to positive ones. The way how to read SHAP values essentially matches the interpretation of regression coefficients in statistical models.

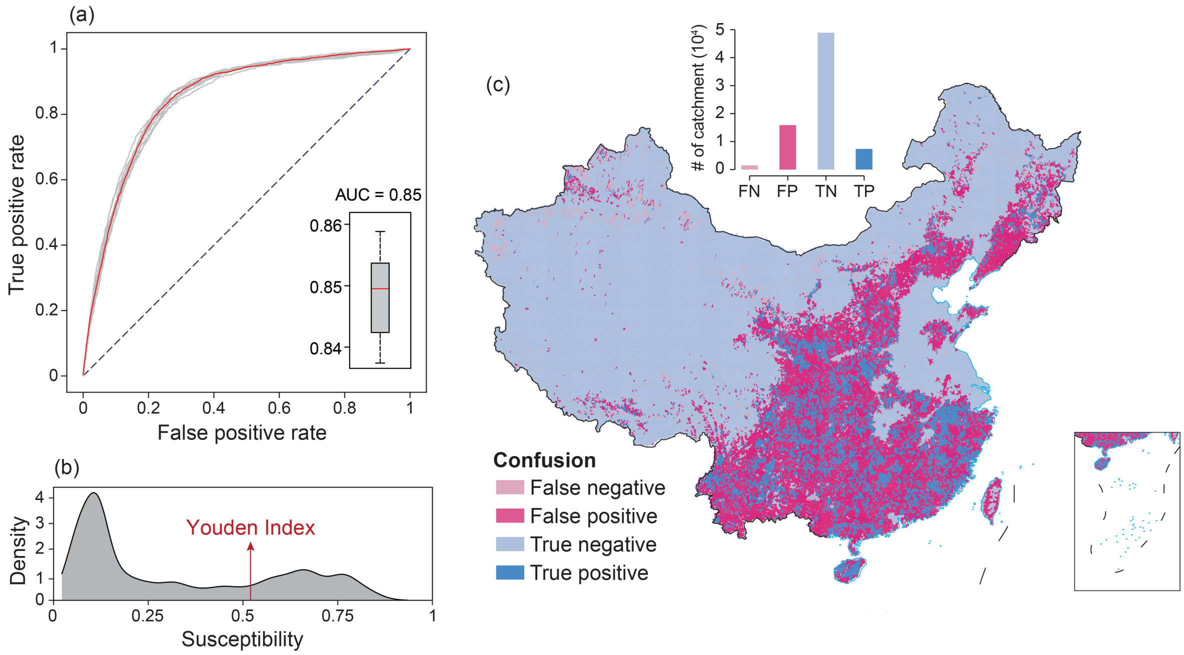

Figure 4: The ROC curves (a) and confusion map (b) for the validation model.

The magnitude of the SHAP value indicates the influence on the final susceptibility whereas the sign indicates whether the given predictor contributes to increasing or decreasing the probability estimates. For instance, most of the predictors have a positive contribution to the pattern of relative probabilities in space. This is not the case for the elongation rate (Er) of the catchment as well as the planar (Plc) and profile (Prc) curvatures.

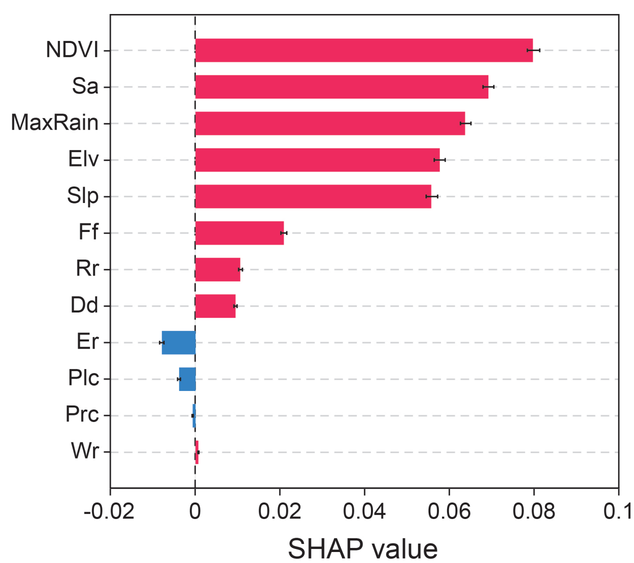

Figure 5: Variable importance expressed in terms of SHAP values.

An additional solution to assess variable contribution in traditional machine learning consists of response plots (e.g., Park, 2015). Here we also produce an analogous illustration but again as a function of SHAP values. Specifically, we plot the SHAP estimates against the normalized variables' domain for each catchment and for each predictor under consideration. This is shown in Figure 6, where the resulting scatterplots present the marginal effects (assuming all other covariate effects to be fixed) adding another dimension to the static view offered by the variable importance. Here we can distinguish portions of each variable domain and how they individually contribute to increasing or decreasing the susceptibility. For instance, NDVI, maximum daily rainfall, and form factor revealed a weak positive effect on the HMP occurrences, whereas the elongation ratio showed a slightly negative association with HMPs.

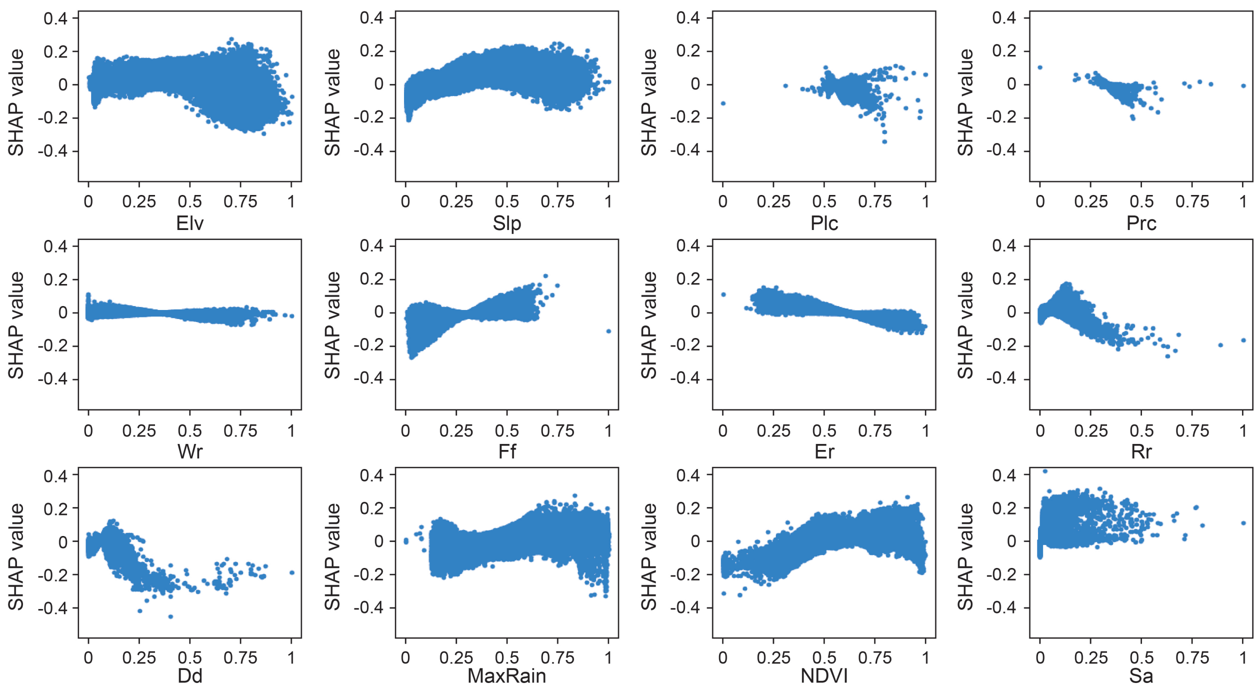

Figure 6: Scatter plots for each variable used in the model.

This plot essentially corresponds to the limit of model explainability of traditional machine learning studies. The next session is dedicated to further exploring predictors' effects and understanding their contribution to the HMP susceptibility model.

4.2.2 Local interpretation

The first step to deepen our understanding of the model results focuses on moving from global to individual catchment predictions. Figure 7 illustrates an intermediate level between the two options by plotting SHAP values for each normalized predictor domain. This further adds another exploratory dimension by plotting the actual susceptibility estimate for each catchment in a violin plot. In such a way, one can quickly visualize whether a given predictor behaves linearly or not. For instance, the elongation ratio shows high susceptibility values on the left side of the violin plot, transitioning to low probabilities at greater elongation ratio values. Conversely, elevation is initially associated with high susceptibility, then moves to non-susceptible catchments and transitions to the right side of the violin to high susceptibility once more.

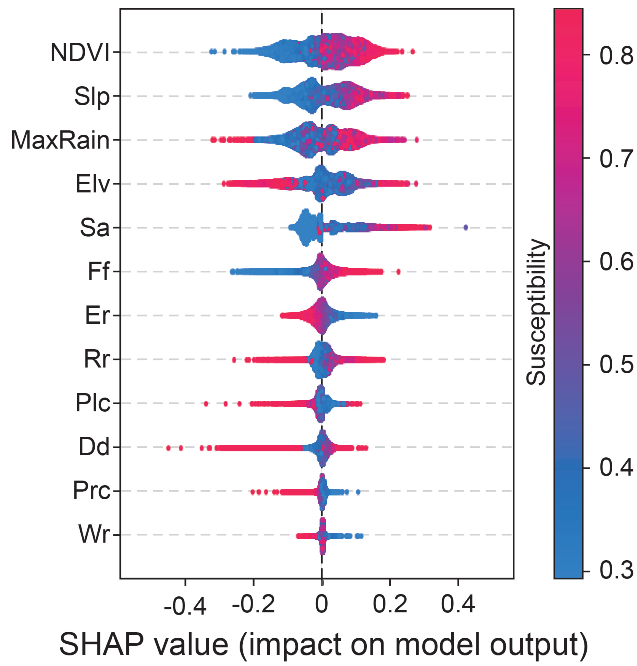

Figure 7: The SHAP value distribution for each variable against the susceptibility. Each dot corresponding to a specific catchment, the color map showed the final susceptibility.

Figure 8 is the first level of localized interpretation of the model results. This plot is built by showing the base and final probabilities for two random catchments, highlighting how each predictor has contributed to the final susceptibility estimate. We recall here that the base probability value is analogous to a model intercept for a statistical model and its definition depends on the proportion of presence/absence data across the whole study area (see, Frattini *et al.*, 2010; Petschko *et al.*, 2014). For instance, panels (a) and (b) both start from the same probability value of 0.32 and respectively reach a final susceptibility of 0.21 and 0.52. The magnitude and sign of each predictor contributing to this value change are colorcoded in the figure, with the actual numerical variation written to further improve readability. It is important to stress that the same variable does not bring the same level of change to the two catchments. For instance, Er has a much larger contribution in panel (a) than it has in panel (b). This is a characteristic of SHAP values, as they essentially visualize the combinations of predictor weight and relative predictor value for each individual mapping unit. As explanatory as this illustration may be, it is difficult to use this level of detail for each catchment.

For this reason, another level of model exploration is offered by computing the combination of each predictor contribution and plotting the ranked probability from the base value

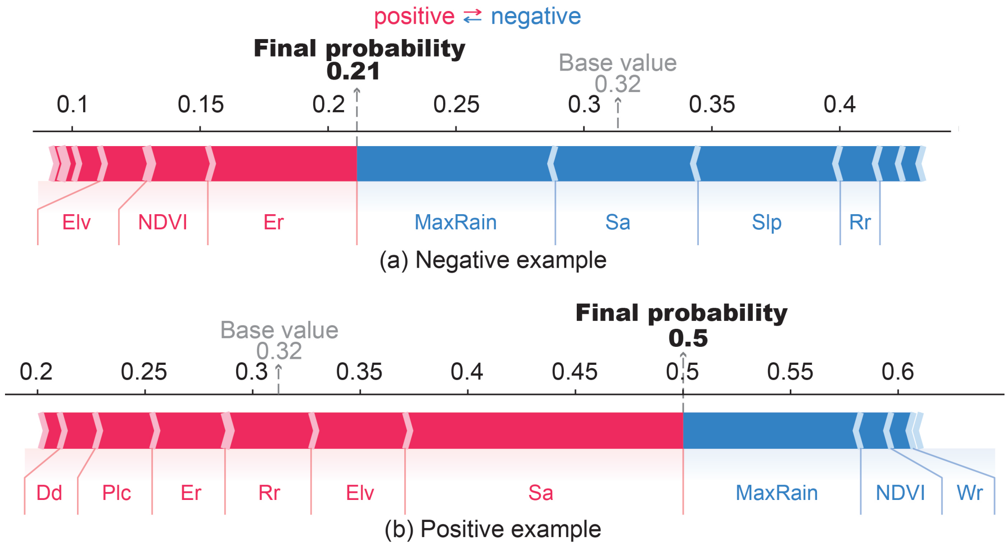

Figure 8: Examples of catchments that were detected as the negative (a) and positive (b) ones.

to the final one, for each catchment. This provides an alternative option for end users to look into how the susceptibility varies, and for the whole Chinese HMP susceptibility, this can be visualized in Figure 9. Implications of the information conveyed will be presented in Section 5.

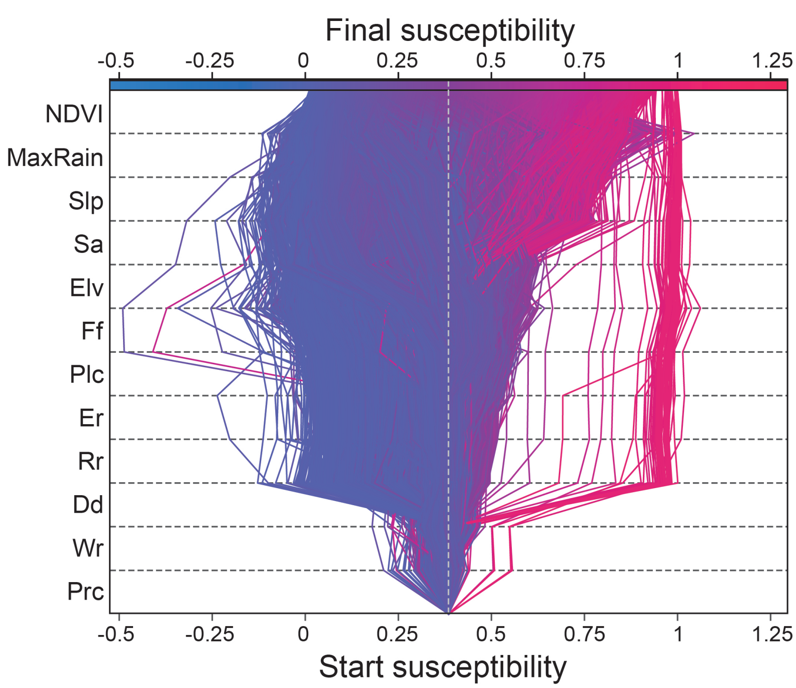

Figure 9: The variation of the probability estimates for all catchments partitioning the study area.

So far, this level of model explainability was already presented in three recent articles (Collini *et al.*, 2022; Zhang *et al.*, 2023; Dahal and Lombardo, 2022). However, what they all missed is translating the information offered by the SHAP values across the geographic space, which is what we will present in the next section.

4.3 Geographic view of predictors' effects

As mentioned above, the strength of using SHAP seen so far for model explainability can be taken a step further. Here we propose to do so by looking into the spatial patterns of SHAP values for each predictor. Such a procedure can offer the added value of hierarchically understanding not only the variable at the global and individual catchment level but also exploring relative contributions and how they vary across the Chinese landscape. This is shown in Figure 10. There, with the exception of the wandering ratio, form factor, elongation ratio, and relief ratio, all other variables' impacts on susceptibility showed distinctive spatial patterns. For instance, this is evident in the positive influence of elevation across the Yungui Plateau and Hexi Corridor (Figure 10a). In the most mountainous areas, the slope exhibited a positive impact on HMPs, and in the plain areas, it showed a negative impact (Figure 10b). As for the maximum daily rainfall, a positive contribution can be observed in eastern China (Figure 10j), and a similar pattern can also be detected in the NDVI (Figure 10k).

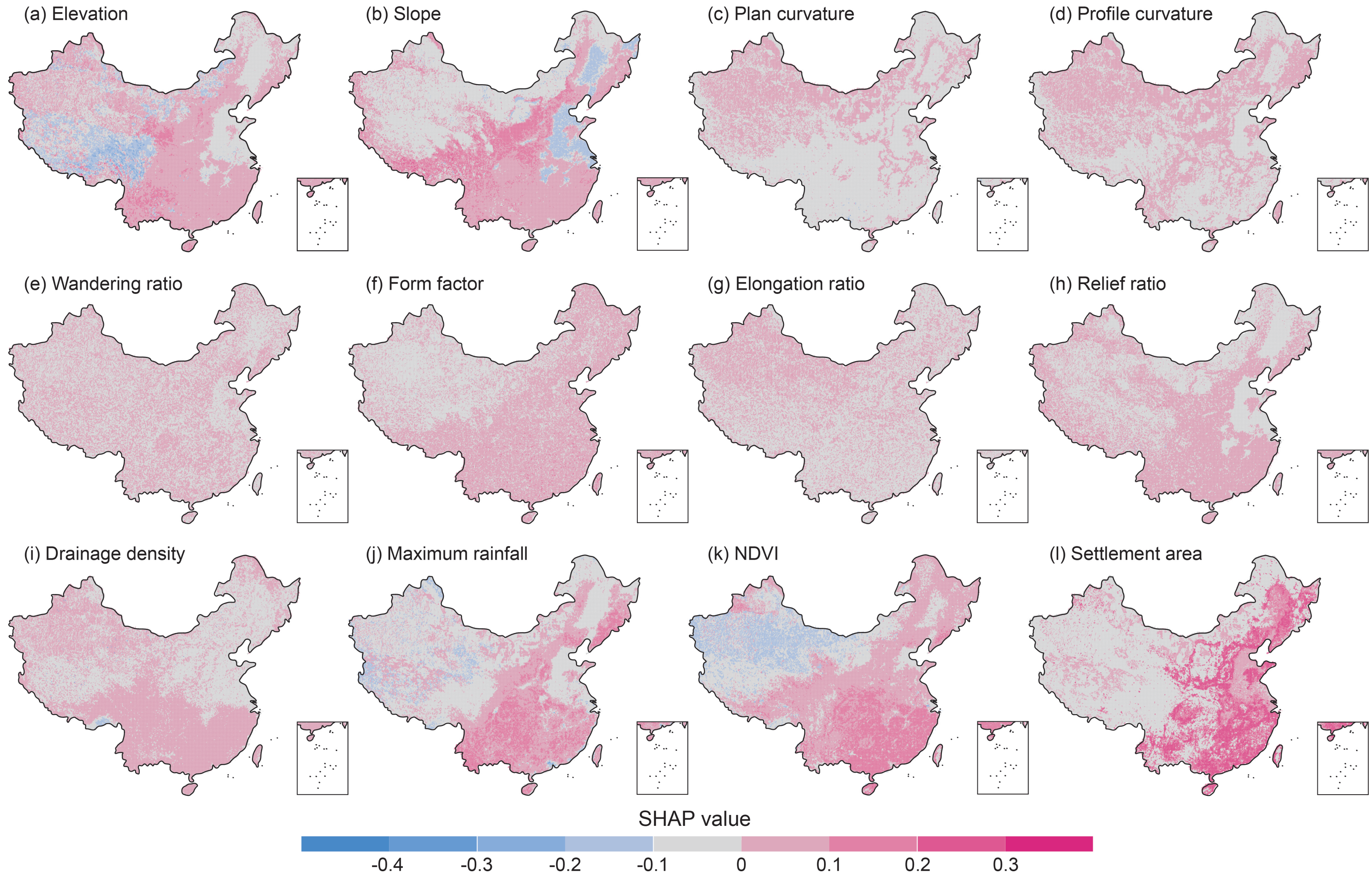

Figure 10: Spatial effects of variables to HMPs detected via the SHAP values, where the pink colors indicate positive contributions and the blue colors represent negative contributions.

The combination of all the exploratory tools we present here is what we believe can become a new standard for the future generation of landslide susceptibility studies.

4.4 Susceptibility mapping

Ultimately, we summarized the resulting susceptibility map for HMPs across the entire Chinese territory in Figure 11. There, we reclassified the susceptibility spectrum, binning the probability values at a decile interval. In general, the areas that present a higher susceptibility are prone to be in southeast China, whereas the low values tend to show in the northwest. However, it is difficult to recognize details in such a vast landscape. For this reason, we also plotted four static zooms, offering a closer view of the susceptibility patterns and the catchment sizes/shapes. Nevertheless, even zooming into the map does not offer a clear view and explainability of the susceptibility estimates. Therefore, we built a webGIS application where each catchment can be queried and the relative SHAP values interactively queried (see, https://arcg.is/0eGGT8).

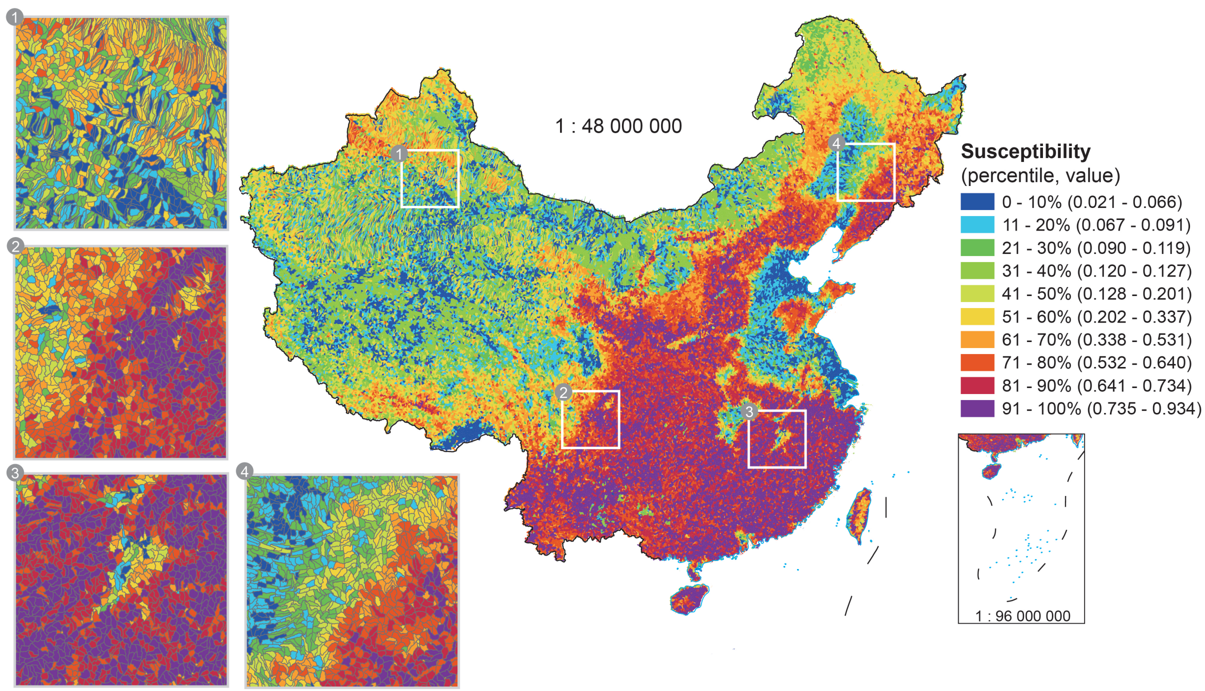

Figure 11: The final mean susceptibility map of HMPs in China.

5 Discussions

5.1 From global to local model interpretations

Standard approaches to understanding why machine learning models return certain outputs are generally based on variable importance ranks. In this contribution, we stress how important it is to extend this traditional view to welcome the SHAP-oriented model explanation instead. The main reason behind this has to do with the static view that variable importance plots offer. Conversely, SHAP-based graphics expand toward variable interaction processes, adding another dimension to the explainability potential of machine learning solutions. This becomes clear in Figure 9, where a closer inspection highlights a cluster of catchments with final susceptibility close to 1. These catchments all start from the same starting point as all others (susceptibility = 0.32), but their predicted value stays essentially the same because of the Dd influence. We recall here that Dd stands for drainage density, whose dominant effect can be geomorphologically justified. As for how this parameter specifically contributes on an individual catchment basis, one can then dive into graphics such as Figure 8, where the second example purposely reports a catchment where the Dd is responsible for a marginal increase in the final susceptibility. Analogous considerations arise for the other dominant factors, including NDVI, maximum daily rainfall, slope, and settlement area. These results well align with other HMP studies (Ragettli *et al.*, 2017; Zhao *et al.*, 2018). However, as informative as these explainable components may be, they still only offer a non-spatial view of the model output. Therefore, to further enrich the model interpretation, here we demonstrate an additional use of SHAP values. In fact, being SHAPs calculated for individual predictors and for individual mapping units, one can easily translate their combination in map form (see Figure 10). As a result, one can visualize and query a unique spatial pattern for each predictor and assess their effect and consistency/heterogeneity across the geographic space. For instance, the influence of the NDVI was previously shown to be among the most important HMP predictors. In Figure 10k though, the spatial dimension is added to this consideration, showing how its model contribution varies across the landscape, with the largest positive contribution depicted across South China, transitioning to smaller SHAP values in Central and Northeast China. Even such a view though is nothing but a static image of the predictors' contribution. With this idea in mind, we decided to prompt the reviewers in thinking about the potential of spatially querying SHAP values, especially, if this can be done through webGIS applications. At this link https://arcg.is/0eGGT8, we provided an interactive cloud-based platform where we stored all our modeling results. There, each catchment susceptibility can be visualized together with each predictor SHAP value responsible for the local HMP probability. We believe that such a way of summarizing model results can become a future standard for susceptibility modeling, in view of maximizing the opportunities of the digital era for risk assessment. In fact, the webGIS application not only reports model results but also offers the ability to bring information on exposure together. To do so, we used data accessed at this link, https://risk.preventionweb.net/ where information on population density and land economical value is reported at the global scale with a 1km resolution along the coastlines and 5km resolution inland (see also, Koks *et al.*, 2019). The exposure information complements the susceptibility, allowing for risk-oriented considerations. This is shown in Figure 12, where we plot the summary of the population and land value as a function of the predicted HMP probability. The catchments labeled as susceptible that contextually report high population and/or high financial value would represent those that may need further attention for tailored risk mitigation strategies.

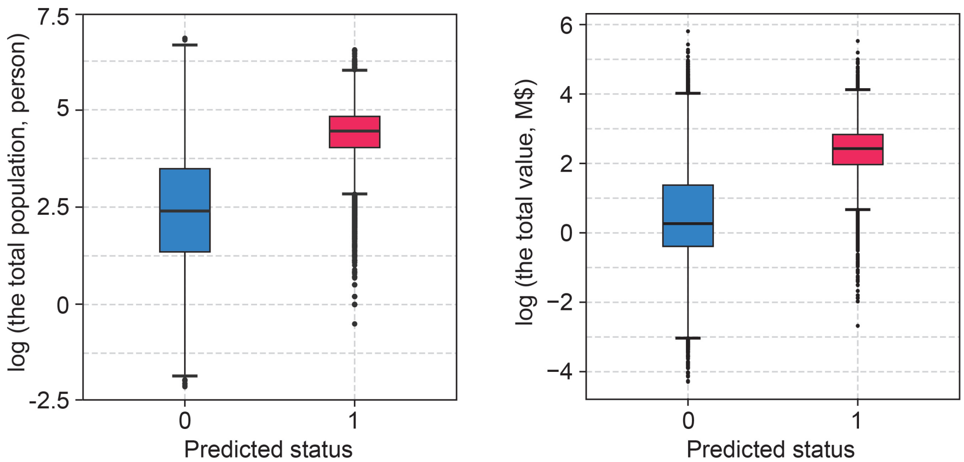

Figure 12: Summary plot of log values of population and land value versus the HMP probability.

5.2 Supporting and opposing arguments

For a long time, despite the higher performance offered by machine learning solutions, statistical models have still represented the preferred alternative for researchers equally interested in comprehending and interpreting why a given data-driven model has produced a certain prediction. Recent advancements in SHAP-explained deep learning modeling have the potential to unify these two fundamental aspects within the very same tool. This is particularly relevant in the context of spatial big data, where machine learning ensures performance, efficiency, and computational speed. For this reason, here we tried to push the boundaries of current explainable AI applications on HMP prediction, testing it over a very large dataset reflecting a continental scale.

The performance and level of interpretation provided, support the choice of this approach. As part of the explainability characteristics, we particularly stress the relevance of converting SHAP values into map form. The resulting geographic view allows for considerations of variable contributions and potential interactions in a straightforward way. This could support decision-making processes, especially if beyond the static map perspective, SHAP values are interactively queried in webGIS applications. The webGIS app we built is meant to showcase these aspects together with considerations of potential HMP risk. In fact, one can dynamically overlay susceptibility estimates, their SHAP corresponding contributors, and exposure information to lay down a comprehensive platform for territorial management and civil protection agencies.

As for the weaknesses behind the experiment we present here, it should be stressed that the temporal component is still missing. Therefore, even putting together HMP susceptibility and exposure data, these are not enough to fully characterize the expected risk but rather constitute an approximation of it. Conversely, the susceptibility model should be extended toward its space-time counterpart (Lombardo *et al.*, 2020; Steger *et al.*, 2022). Such a shift would ensure two possible applications of explainable AI, one where the prediction is performed as a nowcasting/forecasting service for specific events (see also, Collini *et al.*, 2022), and one where its potential can be tapped in for long term scenario-building based on the return time of the HMP trigger.

6 Conclusion

We tested a SHAP-explained deep learning architecture across the whole Chinese territory. Our work showcases a hierarchical overview of predictors' contributions to the final susceptibility, offering both global to local perspectives. The combination of a suite of non-geographic SHAP summaries already represents a step forward compared to traditional alternatives, not only in machine learning but also for the more explainable statistical solutions. This takes another explainable dimension when predictors' effects are examined over the geographic space for individual catchments, something we exemplified in a dedicated webGIS application (accessible at https://arcg.is/0eGGT8) to allow for user interactions. There, we report not only the model results (final HMP susceptibility and SHAP values) but also relevant information on exposure. We believe this modeling approach will constitute the future standard for data-driven solutions not only for HMP but for any natural hazard predictive model. As pointed out in the discussions, we believe risk assessments will be possible once the temporal dimension will be added to the model, something we are already working on.

Acknowledgement

This work was supported by the National Natural Science Foundation of China (grant no. 42201452), the China Postdoctoral Science Foundation (grant no. 2022M710652), and the Fundamental Research Funds for the Central Universities (grant no. 2412022QD003). We especially thank for the support from the China Institute of Water Resources and Hydropower Research (IWHR).

References

Albawi, S., Mohammed, T. A. and Al-Zawi, S. (2017) Understanding of a convolutional neural network. In *2017 International Conference on Engineering and Technology (ICET)*, pp. 1–6.

Aljohani, N. R., Fayoumi, A. and Hassan, S.-U. (2021) A novel focal-loss and class-weight-aware convolutional neural network for the classification of in-text citations. *Journal of Information Science* p. 0165551521991022.

Alvioli, M., Marchesini, I., Pokharel, B., Gnyawali, K. and Lim, S. (2022) Geomorphological slope units of the Himalayas. *Journal of Maps* pp. 1–14.

Amato, G., Eisank, C., Castro-Camilo, D. and Lombardo, L. (2019) Accounting for covariate distributions in slope-unit-based landslide susceptibility models. a case study in the alpine environment. *Engineering Geology* **260**, In print.

Band, S. S., Janizadeh, S., Chandra Pal, S., Saha, A., Chakrabortty, R., Melesse, A. M. and Mosavi, A. (2020) Flash flood susceptibility modeling using new approaches of hybrid and ensemble tree-based machine learning algorithms. *Remote Sensing* **12**(21), 3568.

Baptista, M. L., Goebel, K. and Henriques, E. M. (2022) Relation between prognostics predictor evaluation metrics and local interpretability SHAP values. *Artificial Intelligence* **306**, 103667.

Brenning, A. (2005) Spatial prediction models for landslide hazards: review, comparison and evaluation. *Natural Hazards and Earth System Science* **5**(6), 853–862.

Brenning, A. (2008) Statistical geocomputing combining R and SAGA: The example of landslide susceptibility analysis with generalized additive models. *Hamburger Beiträge zur Physischen Geographie und Landschaftsökologie* **19**(23-32), 410.

Bui, D. T., Hoang, N.-D., Martínez-Álvarez, F., Ngo, P.-T. T., Hoa, P. V., Pham, T. D., Samui, P. and Costache, R. (2020) A novel deep learning neural network approach for predicting flash flood susceptibility: A case study at a high frequency tropical storm area. *Science of The Total Environment* **701**, 134413.

Camilo, D. C., Lombardo, L., Mai, P. M., Dou, J. and Huser, R. (2017) Handling high predictor dimensionality in slope-unit-based landslide susceptibility models through LASSO-penalized Generalized Linear Model. *Environmental Modelling & Software* **97**, 145–156.

Can, T., Nefeslioglu, H. A., Gokceoglu, C., Sonmez, H. and Duman, T. Y. (2005) Susceptibility assessments of shallow earthflows triggered by heavy rainfall at three catchments by logistic regression analyses. *Geomorphology* **72**(1-4), 250–271.

Carrara, A., Cardinali, M., Guzzetti, F. and Reichenbach, P. (1995) Gis technology in mapping landslide hazard. In *Geographical Information Systems in Assessing Natural Hazards*, Advances in Natural and Technological Hazards Research, pp. 135–175. Dordrecht: Kluwer, Springer. ISBN 978-90-481-4561-4 978-94-015-8404-3.

Carrara, A., Crosta, G. and Frattini, P. (2008) Comparing models of debris-flow susceptibility in the alpine environment. *Geomorphology* **94**(3-4), 353–378.

Collini, E., Palesi, L. I., Nesi, P., Pantaleo, G., Nocentini, N. and Rosi, A. (2022) Predicting and understanding landslide events with explainable AI. *IEEE Access* **10**, 31175–31189.

Dahal, A. and Lombardo, L. (2022) Explainable artificial intelligence in geoscience: a glimpse into the future of landslide susceptibility modeling .

De Villiers, J. and Barnard, E. (1993) Backpropagation neural nets with one and two hidden layers. *IEEE Transactions on Neural Networks* **4**(1), 136–141.

Domeneghetti, A., Vorogushyn, S., Castellarin, A., Merz, B. and Brath, A. (2013) Probabilistic flood hazard mapping: effects of uncertain boundary conditions. *Hydrology and Earth System Sciences* **17**(8), 3127–3140.

Fell, R., Corominas, J., Bonnard, C., Cascini, L., Leroi, E., Savage, W. Z. *et al.* (2008) Guidelines for landslide susceptibility, hazard and risk zoning for land-use planning. *Engineering Geology* **102**(3-4), 99–111.

Fluss, R., Faraggi, D. and Reiser, B. (2005) Estimation of the Youden Index and its associated cutoff point. *Biometrical Journal: Journal of Mathematical Methods in Biosciences* **47**(4), 458–472.

Fotheringham, A. S., Brunsdon, C. and Charlton, M. (2003) *Geographically weighted regression: the analysis of spatially varying relationships*. John Wiley & Sons.

Frattini, P., Crosta, G. and Carrara, A. (2010) Techniques for evaluating the performance of landslide susceptibility models. *Engineering Geology* **111**(1), 62–72.

Gariano, S. L. and Guzzetti, F. (2016) Landslides in a changing climate. *Earth-Science Reviews* **162**, 227–252.

Goetz, J., Brenning, A., Petschko, H. and Leopold, P. (2015) Evaluating machine learning and statistical prediction techniques for landslide susceptibility modeling. *Computers & Geosciences* **81**, 1–11.

Gunning, D. (2017) Explainable artificial intelligence (xai). *Defense Advanced Research Projects Agency (DARPA), nd Web* **2**(2), 1.

Guzzetti, F., Reichenbach, P., Ardizzone, F., Cardinali, M. and Galli, M. (2006) Estimating the quality of landslide susceptibility models. *Geomorphology* **81**(1-2), 166–184.

He, B., Huang, X., Ma, M., Chang, Q., Tu, Y., Li, Q., Zhang, K. and Hong, Y. (2018) Analysis of flash flood disaster characteristics in China from 2011 to 2015. *Natural Hazards* **90**, 407–420.

Horton, R. E. (1932) Drainage-basin characteristics. *Transactions, American Geophysical Union* **13**(1), 350–361.

Hosmer Jr, D. W., Lemeshow, S. and Sturdivant, R. X. (2013) *Applied logistic regression.* Volume 398. John Wiley & Sons.

Hosseini, F. S., Choubin, B., Mosavi, A., Nabipour, N., Shamshirband, S., Darabi, H. and Haghighi, A. T. (2020) Flash-flood hazard assessment using ensembles and Bayesian-based machine learning models: Application of the simulated annealing feature selection method. *Science of the Total Environment* **711**, 135161.

Jacobs, L., Kervyn, M., Reichenbach, P., Rossi, M., Marchesini, I., Alvioli, M. and Dewitte, O. (2020) Regional susceptibility assessments with heterogeneous landslide information: Slope unit-vs. pixel-based approach. *Geomorphology* **356**, 107084.

Kern, A. N., Addison, P., Oommen, T., Salazar, S. E. and Coffman, R. A. (2017) Machine learning based predictive modeling of debris flow probability following wildfire in the intermountain Western United States. *Mathematical Geosciences* **49**, 717–735.

Kobiyama, M. and Goerl, R. F. (2007) Quantitative method to distinguish flood and flash flood as disasters. *SUISUI Hydrological Research Letters* **1**, 11–14.

Koks, E. E., Rozenberg, J., Zorn, C., Tariverdi, M., Vousdoukas, M., Fraser, S. A., Hall, J. and Hallegatte, S. (2019) A global multi-hazard risk analysis of road and railway infrastructure assets. *Nature Communications* **10**(1), 2677.

Korup, O. and Stolle, A. (2014) Landslide prediction from machine learning. *Geology Today* **30**(1), 26–33.

Li, Y. and Yuan, Y. (2017) Convergence analysis of two-layer neural networks with relu activation. *Advances in Neural Information Processing Systems* **30**.

Li, Z. (2022) Extracting spatial effects from machine learning model using local interpretation method: An example of SHAP and XGBoost. *Computers, Environment and Urban Systems* **96**, 101845.

Lima, P., Steger, S., Glade, T. and Murillo-García, F. G. (2022) Literature review and bibliometric analysis on data-driven assessment of landslide susceptibility. *Journal of Mountain Science* **19**(6), 1670–1698.

Lin, Q., Lima, P., Steger, S., Glade, T., Jiang, T., Zhang, J., Liu, T. and Wang, Y. (2021) National-scale data-driven rainfall induced landslide susceptibility mapping for China by accounting for incomplete landslide data. *Geoscience Frontiers* **12**(6), 101248.

Lin, Q., Steger, S., Pittore, M., Zhang, J., Wang, L., Jiang, T. and Wang, Y. (2022) Evaluation of potential changes in landslide susceptibility and landslide occurrence frequency in China under climate change. *Science of the Total Environment* **850**, 158049.

Liu, C., Guo, L., Ye, L., Zhang, S., Zhao, Y. and Song, T. (2018a) A review of advances in China's flash flood early-warning system. *Natural Hazards* **92**(2), 619–634.

Liu, Y., Huang, Y., Wan, J., Yang, Z. and Zhang, X. (2021) Analysis of human activity impact on flash floods in China from 1950 to 2015. *Sustainability* **13**(1), 217.

Liu, Y., Yang, Z., Huang, Y. and Liu, C. (2018b) Spatiotemporal evolution and driving factors of China's flash flood disasters since 1949. *Science China Earth Sciences* **61**(12), 1804–1817.

Loche, M., Alvioli, M., Marchesini, I., Bakka, H. and Lombardo, L. (2022a) Landslide susceptibility maps of Italy: Lesson learnt from dealing with multiple landslide types and the uneven spatial distribution of the national inventory. *Earth-Science Reviews* p. 104125.

Loche, M., Scaringi, G., Yunus, A. P., Catani, F., Tanyaş, H., Frodella, W., Fan, X. and Lombardo, L. (2022b) Surface temperature controls the pattern of post-earthquake landslide activity. *Scientific Reports* **12**(1), 988.

Lombardo, L., Bakka, H., Tanyas, H., van Westen, C., Mai, P. M. and Huser, R. (2019) Geostatistical modeling to capture seismic-shaking patterns from earthquake-induced landslides. *Journal of Geophysical Research: Earth Surface* **124**(7), 1958–1980.

Lombardo, L. and Mai, P. M. (2018) Presenting logistic regression-based landslide susceptibility results. *Engineering Geology* **244**, 14–24.

Lombardo, L., Opitz, T., Ardizzone, F., Guzzetti, F. and Huser, R. (2020) Space-time landslide predictive modelling. *Earth-Science Reviews* p. 103318.

Lubo-Robles, D., Devegowda, D., Jayaram, V., Bedle, H., Marfurt, K. J. and Pranter, M. J. (2020) Machine learning model interpretability using SHAP values: Application to a seismic facies classification task. In *SEG International Exposition and Annual Meeting.*

Lundberg, S. M. and Lee, S.-I. (2017) A Unified Approach to Interpreting Model Predictions. In *Advances in Neural Information Processing Systems 30*, eds I. Guyon, U. V. Luxburg, S. Bengio, H. Wallach, R. Fergus, S. Vishwanathan and R. Garnett, pp. 4765–4774. Curran Associates, Inc.

Marchi, L., Borga, M., Preciso, E. and Gaume, E. (2010) Characterisation of selected extreme flash floods in Europe and implications for flood risk management. *Journal of Hydrology* **394**(1-2), 118–133.

Merghadi, A., Yunus, A. P., Dou, J., Whiteley, J., ThaiPham, B., Bui, D. T., Avtar, R. and Abderrahmane, B. (2020) Machine learning methods for landslide susceptibility studies: A comparative overview of algorithm performance. *Earth-Science Reviews* p. 103225.

Merz, B., Elmer, F. and Thieken, A. (2009) Significance of "high probability/low damage" versus "low probability/high damage" flood events. *Natural Hazards and Earth System Sciences* **9**(3), 1033–1046.

Molnar, C. (2020) *Interpretable machine learning*. Lulu. com.

Moreira, A., Krieger, G., Hajnsek, I., Hounam, D., Werner, M., Riegger, S. and Settelmeyer, E. (2004) TanDEM-X: a TerraSAR-X add-on satellite for single-pass SAR interferometry. In *IGARSS 2004. 2004 IEEE International Geoscience and Remote Sensing Symposium*, volume 2, pp. 1000–1003.

Nicu, I. C., Elia, L., Rubensdotter, L., Tanyaş, H. and Lombardo, L. (2023) Multi-hazard susceptibility mapping of cryospheric hazards in a high-Arctic environment: Svalbard Archipelago. *Earth System Science Data* **15**(1), 447–464.

Opitz, T., Bakka, H., Huser, R. and Lombardo, L. (2022) High-resolution bayesian mapping of landslide hazard with unobserved trigger event. *The Annals of Applied Statistics* **16**(3), 1653–1675.

Ozdemir, A. (2009) Landslide susceptibility mapping of vicinity of Yaka Landslide (Gelendost, Turkey) using conditional probability approach in GIS. *Environmental Geology* **57**, 1675–1686.

Panahi, M., Jaafari, A., Shirzadi, A., Shahabi, H., Rahmati, O., Omidvar, E., Lee, S. and Bui, D. T. (2021) Deep learning neural networks for spatially explicit prediction of flash flood probability. *Geoscience Frontiers* **12**(3), 101076.

Panati, C., Wagner, S. and Brüggenwirth, S. (2022) Feature Relevance Evaluation using Grad-CAM, LIME and SHAP for Deep Learning SAR Data Classification. In *2022 23rd International Radar Symposium (IRS)*, pp. 457–462.

Park, N.-W. (2015) Using maximum entropy modeling for landslide susceptibility mapping with multiple geoenvironmental data sets. *Environmental Earth Sciences* **73**, 937–949.

Petschko, H., Brenning, A., Bell, R., Goetz, J. and Glade, T. (2014) Assessing the quality of landslide susceptibility maps—case study lower austria. *Natural Hazards and Earth System Sciences* **14**(1), 95–118.

Ragettli, S., Zhou, J., Wang, H., Liu, C. and Guo, L. (2017) Modeling flash floods in ungauged mountain catchments of China: A decision tree learning approach for parameter regionalization. *Journal of Hydrology* **555**, 330–346.

Ramyachitra, D. and Manikandan, P. (2014) Imbalanced dataset classification and solutions: a review. *International Journal of Computing and Business Research (IJCBR)* **5**(4), 1–29.

Reichenbach, P., Rossi, M., Malamud, B. D., Mihir, M. and Guzzetti, F. (2018) A review of statistically-based landslide susceptibility models. *Earth-Science Reviews* **180**, 60–91.

Ribeiro, M. T., Singh, S. and Guestrin, C. (2016) "why should i trust you?" explaining the predictions of any classifier. In *Proceedings of the 22nd ACM SIGKDD International Conference on Knowledge Discovery and Data Mining*, pp. 1135–1144.

Roshan, K. and Zafar, A. (2022) Using Kernel SHAP XAI Method to Optimize the Network Anomaly Detection Model. In *2022 9th International Conference on Computing for Sustainable Global Development (INDIACom)*, pp. 74–80.

Samek, W., Wiegand, T. and Müller, K.-R. (2017) Explainable artificial intelligence: Understanding, visualizing and interpreting deep learning models. *arXiv preprint arXiv:1708.08296* .

Santangelo, N., Santo, A., Di Crescenzo, G., Foscari, G., Liuzza, V., Sciarrotta, S. and Scorpio, V. (2011) Flood susceptibility assessment in a highly urbanized alluvial fan: the case study of Sala Consilina (southern Italy). *Natural Hazards and Earth System Sciences* **11**(10), 2765–2780.

Schumm, S. A. (1956) Evolution of drainage systems and slopes in badlands at Perth Amboy, New Jersey. *Geological Society of America Bulletin* **67**(5), 597–646.

Shirzadi, A., Shahabi, H., Chapi, K., Bui, D. T., Pham, B. T., Shahedi, K. and Ahmad, B. B. (2017) A comparative study between popular statistical and machine learning methods for simulating volume of landslides. *Catena* **157**, 213–226.

Shrikumar, A., Greenside, P. and Kundaje, A. (2017) Learning important features through propagating activation differences. In *International Conference on Machine Learning*, pp. 3145–3153.

Singh, A., Sengupta, S. and Lakshminarayanan, V. (2020) Explainable deep learning models in medical image analysis. *Journal of Imaging* **6**(6), 52.

Song, C., Shi, X. and Wang, J. (2020) Spatiotemporally varying coefficients (stvc) model: A bayesian local regression to detect spatial and temporal nonstationarity in variables relationships. *Annals of GIS* **26**(3), 277–291.

Steger, S., Moreno, M., Crespi, A., Zellner, P. J., Gariano, S. L., Brunetti, M. T., Melillo, M., Peruccacci, S., Marra, F., Kohrs, R. *et al.* (2022) Deciphering seasonal effects of triggering and preparatory precipitation for improved shallow landslide prediction using generalized additive mixed models. *Natural Hazards and Earth System Sciences Discussions* pp. 1–38.

Strahler, A. N. (1952) Dynamic basis of geomorphology. *Geological Society of America Bulletin* **63**(9), 923–938.

Štrumbelj, E. and Kononenko, I. (2014) Explaining prediction models and individual predictions with feature contributions. *Knowledge and Information Systems* **41**, 647–665.

Tehrani, F. S., Calvello, M., Liu, Z., Zhang, L. and Lacasse, S. (2022) Machine learning and landslide studies: recent advances and applications. *Natural Hazards* **114**(2), 1197–1245.

Titti, G., Napoli, G. N., Conoscenti, C. and Lombardo, L. (2022) Cloud-based interactive susceptibility modeling of gully erosion in Google Earth Engine. *International Journal of Applied Earth Observation and Geoinformation* **115**, 103089.

Townsend, J. T. (1971) Theoretical analysis of an alphabetic confusion matrix. *Perception & Psychophysics* **9**, 40–50.

Ullah, I., Liu, K., Yamamoto, T., Zahid, M. and Jamal, A. (2023) Modeling of machine learning with shap approach for electric vehicle charging station choice behavior prediction. *Travel Behaviour and Society* **31**, 78–92.

Wang, D., Thunéll, S., Lindberg, U., Jiang, L., Trygg, J. and Tysklind, M. (2022a) Towards better process management in wastewater treatment plants: Process analytics based on SHAP values for tree-based machine learning methods. *Journal of Environmental Management* **301**, 113941.

Wang, N., Cheng, W., Lombardo, L., Xiong, J. and Guo, L. (2021) Statistical spatiotemporal analysis of hydro-morphological processes in China during 1950–2015. *Stochastic Environmental Research and Risk Assessment* pp. 1–21.

Wang, N., Cheng, W., Marconcini, M., Bachofer, F., Liu, C., Xiong, J. and Lombardo, L. (2022b) Space-time susceptibility modeling of hydro-morphological processes at the Chinese national scale. *Engineering Geology* **301**, 106586.

Wang, N., Cheng, W., Wang, B., Liu, Q. and Zhou, C. (2020) Geomorphological regionalization theory system and division methodology of China. *Journal of Geographical Sciences* **30**(2), 212–232.

Xiong, J., Li, J., Cheng, W., Wang, N. and Guo, L. (2019) A GIS-based support vector machine model for flash flood vulnerability assessment and mapping in China. *ISPRS International Journal of Geo-Information* **8**(7), 297.

Xiong, J., Pang, Q., Cheng, W., Wang, N. and Yong, Z. (2020) Reservoir risk modelling using a hybrid approach based on the feature selection technique and ensemble methods. *Geocarto International* pp. 1–22.

Yeon, Y.-K., Han, J.-G. and Ryu, K. H. (2010) Landslide susceptibility mapping in Injae, Korea, using a decision tree. *Engineering Geology* **116**(3-4), 274–283.

Yilmaz, I. (2009) Landslide susceptibility mapping using frequency ratio, logistic regression, artificial neural networks and their comparison: a case study from Kat landslides (Tokat—Turkey). *Computers & Geosciences* **35**(6), 1125–1138.

Yu, L., Porwal, A., Holden, E.-J. and Dentith, M. C. (2012) Towards automatic lithological classification from remote sensing data using support vector machines. *Computers & Geosciences* **45**, 229–239.

Zhang, J., Ma, X., Zhang, J., Sun, D., Zhou, X., Mi, C. and Wen, H. (2023) Insights into geospatial heterogeneity of landslide susceptibility based on the SHAP-XGBoost model. *Journal of Environmental Management* **332**, 117357.

Zhao, G., Liu, R., Yang, M., Tu, T., Ma, M., Hong, Y. and Wang, X. (2022a) Large-scale flash flood warning in China using deep learning. *Journal of Hydrology* **604**, 127222.

Zhao, G., Pang, B., Xu, Z., Yue, J. and Tu, T. (2018) Mapping flood susceptibility in mountainous areas on a national scale in China. *Science of the Total Environment* **615**, 1133–1142.

Zhao, P., Masoumi, Z., Kalantari, M., Aflaki, M. and Mansourian, A. (2022b) A GIS-based landslide susceptibility mapping and variable importance analysis using artificial intelligent training-based methods. *Remote Sensing* **14**(1), 211.